



LAWRENCE
LIVERMORE
NATIONAL
LABORATORY

Transmission Electron Microscopy Characterization of Helium Bubbles in Aged Plutonium

A. J. Schwartz, M. A. Wall, T. G. Zocco, K. J. M.
Blobaum

November 5, 2004

Materialovedenie

Disclaimer

This document was prepared as an account of work sponsored by an agency of the United States Government. Neither the United States Government nor the University of California nor any of their employees, makes any warranty, express or implied, or assumes any legal liability or responsibility for the accuracy, completeness, or usefulness of any information, apparatus, product, or process disclosed, or represents that its use would not infringe privately owned rights. Reference herein to any specific commercial product, process, or service by trade name, trademark, manufacturer, or otherwise, does not necessarily constitute or imply its endorsement, recommendation, or favoring by the United States Government or the University of California. The views and opinions of authors expressed herein do not necessarily state or reflect those of the United States Government or the University of California, and shall not be used for advertising or product endorsement purposes.

Transmission Electron Microscopy Characterization of Helium Bubbles in Aged Plutonium

A.J. Schwartz,^{1*} M.A. Wall,¹ T.G. Zocco,² and K.J.M. Blobaum¹

¹Lawrence Livermore National Laboratory, Livermore, California 94550, USA

²Los Alamos National Laboratory, Los Alamos, New Mexico 87545, USA

*Email: schwartz6@llnl.gov

Abstract

The self-irradiation damage generated by alpha decay of plutonium results in the formation of lattice defects, helium, and uranium atoms. Over time, microstructural evolution resulting from the self-irradiation may influence the physical and mechanical properties of the material. In order to assess microstructural changes, we have developed and applied procedures for the specimen preparation, handling, and transmission electron microscopy characterization of Pu alloys. These transmission electron microscopy investigations of Pu-Ga alloys ranging in age up to 42-years old reveal the presence of nanometer-sized helium bubbles. The number density of bubbles and the average size have been determined for eight different aged materials.

Introduction

The characterization and modeling of microstructural changes in aging plutonium alloys is an important aspect of the nuclear Stockpile Stewardship Program. Dimensional changes in Pu alloys may result from three different phenomena: the initial transient, helium accumulation, and void swelling. The initial transient is a well-known effect that results from the initial cascade damage.¹ The cascade damage results in the formation of dislocation loops that lead to changes in lattice parameters and tends to saturate within a few years. The second contributor to dimensional change is the build-up of helium from alpha decay.² The third possible age-related phenomenon is void swelling,³ but this has not yet been observed in naturally aged Pu alloys. Our goal in the utilization of transmission electron microscopy (TEM) is to characterize any potential change in the microstructure as a function of the age of the Pu alloys.

The self-irradiation of ^{239}Pu lies at the center of the age-related microstructural changes. The radioactive decay of Pu, primarily in the form of alpha decay, transmutes the Pu atom into a U atom and an alpha particle. Radiation damage from alpha decay in plutonium occurs at a rate of ~ 0.1 dpa/yr (displacements per atom per year). Calculations have shown that the 86keV ^{235}U recoil traverses the lattice approximately 12 nm and results in the formation of approximately 2300 Frenkel pairs. Although 90% of these Frenkel pairs return to their initial lattice sites within the first 200 nanoseconds, the remaining 10% remain in the lattice in the form of free interstitials and vacancies or interstitial or vacancy clusters.^{4,5} It is well known in the nuclear reactor community that these microstructural changes ultimately result in property changes that include void swelling, mechanical hardening, and reduction in ductility.

On the other side of the alpha decay, a 5 MeV alpha particle traverses the lattice approximately 10 μm , slowly losing its energy via electronic excitations before coming to rest with the generation of an additional 265 Frenkel pairs. The alpha particle picks up two electrons to become a He atom, leading to a helium generation rate of approximately 41 atomic parts per million per year. Positron annihilation data by Howell et al.⁶ indicate that the He atom immediately finds an unfilled vacancy. After annealing at 400°C for 1 hour, Rohr et al.,⁷ Rohr and Staudhammer,⁸ and Zocco and Rohr⁹ showed that 17-year aged Pu alloy samples have a significant population of bubbles observable with TEM. It is believed that the high temperature heat treatment allowed for diffusion and migration of the helium atoms, leading to bubble formation inside the crystalline matrix and along grain boundaries. Wolfer⁴ predicted the formation of He bubbles in naturally aged (not annealed) Pu, but until this investigation, no He bubbles had been observed in naturally aged Pu.

Sample preparation and transmission electron microscopy characterization of plutonium alloys are technically challenging due to the toxicity, radioactivity, and high oxidation rate of Pu. The toxicity and radioactivity of Pu pose a major health hazard and a significant investment of time, money, and engineering is required to mitigate these hazards so that one can safely prepare and transfer specimens for observation in the TEM. The oxidation rate of the sample is related to the specimen preparation parameters, the amount of time required to move the sample to TEM, and the environment that the specimen is exposed to during the transfer process. The oxidation can easily preclude the observation of metallic Pu in the TEM by masking the Pu metal under a thick oxide film or transforming the metal entirely to

oxide. Additionally, oxide formation and the spalling of oxide from the specimen represent the primary mechanism for the dispersal of radioactive materials, which poses a major health risk.

In this report, we will describe the procedures that we have developed for the safe handling, preparation, and transfer of Pu specimens and the results of the transmission electron microscopy characterization. To date, numerous specimens with minimal oxide have been safely handled and observed in the TEM with no radioactive contamination to the external parts of the specimen holder, personnel, or facilities. Furthermore, radiological surveys of the internal parts of the TEM have not revealed any contamination. Only the internal surfaces and surrounding regions of the specimen cup show signs of fixed contamination.

As with any TEM investigation, proper sample preparation is of utmost importance. The ability to prepare electron transparent regions without specimen preparation induced artifacts facilitates TEM investigation over many length scales of microstructure. This is particularly true for Pu where the maximum relative viewable thickness is 50% that of Cu and less than 20% that of Al.

Experimental Equipment

In order to facilitate safe handling and sample preparation, an inert atmosphere, recirculating glove box was purchased and installed in a radioactive materials handling laboratory. The glove box achieves a baseline reading of ≈ 0.2 ppm O_2 and ≈ 1 ppm H_2O with an inert atmosphere of nitrogen. Within the glove box, we have installed a slow speed diamond saw for slicing, a lapping machine for automated lapping and metallographic polishing, a hand lapping device for manual TEM lapping, a metallograph with digital imaging, and a TEM electropolishing cell. The glove box has feed-throughs for the electrical connections to the electropolishing power supply and a computer for image acquisition on the metallograph. Supplies and samples are moved into and out of the glove box via an antechamber. The antechamber can be either evacuated or purged with nitrogen so the passing of materials into and out of the glove box will minimally affect the inert atmosphere in the glove box. After samples are sliced, lapped, and electropolished, they are loaded into a vacuum-transfer TEM specimen holder (VTSH). An airlock was constructed on the side of the glove box to allow transfer of the specimen into the specimen holder under

inert atmosphere. The Pu specimen, while under vacuum in the VTSH, is transferred to the airlock of the TEM and inserted into the TEM column. After characterization in the TEM, the specimen is transferred back to the glove box, while still under vacuum in the VTSH.

TEM examinations were initially performed on a JEOL 200CX scanning transmission electron microscope (STEM). After initial sample preparation and safety procedures were proven on the older JEOL 200CX, TEM examinations were carried out on a new Philips CM300FEG with STEM, energy dispersive spectroscopy (EDX) and energy filtering capabilities. This microscope is equipped with a Gatan Imaging Filter and is operated at 300 kV. Standard microscopy such as imaging, diffraction, and spectroscopy can easily be performed.

Experimental Procedure

Bulk material in the form of 2.8-mm diameter cylinders is machined from thin plate material using a milling machine. The cutting speed is < 30.5 m/min, the depth of cut per revolution is ≈ 0.05 mm, and trichloroethylene (TCE) is used as the cutting fluid. These samples are cleaned and packaged under inert atmosphere for transfer to the glove box for TEM sample preparation. The 2.8-mm diameter core is then mounted with DUCO cement onto a slotted aluminum block for slicing. The DUCO cement is allowed to dry at room temperature for a minimum of 60 minutes. Using a 0.152 mm wide diamond blade on a slow speed saw, slices ≈ 0.50 mm wide are cut from the core. The individual slices are dissolved off of the aluminum mount with acetone then remounted using SUPERHOLD glue onto the lapping device. Using successively finer grit lapping films (30, 12 and $3\mu\text{m}$), the first side of the sample is lapped to ≈ 0.38 mm in thickness at intervals of $\approx 10\ \mu\text{m}$. The sample is then dissolved off of the lapping mount using acetone and remounted using SUPERHOLD glue with the first lapped side down. Lapping of the second side of the specimen disc continues using the same lapping sequence as the first side to a final thickness of ≈ 0.200 mm. After lapping is finished, the sample is then dissolved off of the specimen mount and cleaned in acetone. The amounts of material thickness removed for each of the grit sizes are as follows: $30\ \mu\text{m} \approx 0.100$ mm, $12\ \mu\text{m} \approx 0.025$ mm, $3\mu\text{m} \approx 0.013$ mm.

Electropolishing is the next step. A specimen is placed in the electropolishing holder. The specimen holder is placed into the electropolishing cell and allowed to cool in the solution for ≈ 30 seconds. The electropolishing solution composition, by volume, is made

up of 10% nitric acid (70% concentration), 45% methanol and 45% butoxyethanol (butylcellusolve). The parameters for electropolishing are as follows: -20°C , 115V and $\approx 50\text{mA}$. The specimen is thinned continuously to perforation. After perforation, the sample is immediately re-polished at a higher voltage (135V) for 2-3 seconds to remove a thin anodic film that develops during the continuous polishing at lower voltages. The sample is then rinsed in the holder with methanol (anhydrous), removed from the holder, and placed in methanol. The sample is rinsed in several baths of methanol for approximately 1 minute each and it is finally rinsed and stored in 100% ethanol. The finished specimen is very similar in appearance to that of other shiny metal TEM specimens (e.g. Al, stainless steel, etc.).

In preparation for introducing the Pu alloy specimen into the tem, it is removed from the ethanol and loaded into the specimen cup of the VTSH. After the specimen is in place, a 3 mm diameter by 1.5 mm hole Cu grid is placed on top of the specimen. The specimen assembly is held in place by a hex-ring supplied with the VTSH.

The specimen holder is now ready for evacuation and transfer to the TEM. Evacuation and transfer is as follows. A cover slip is placed over the exposed tip of the VTSH in the glove box. The cover slip has been engineered to form a vacuum tight seal over the VTSH to the airlock on the glove box and has a vacuum connection to a high vacuum pumping station. Figure 1 is a schematic drawing of the specimen holder airlock and evacuation system. The specimen holder and cover slip volume are evacuated to a pressure of less than 1 millitorr in less than 2 minutes. While still being evacuated, the specimen tip is retracted back into the main shaft of the specimen holder forming a vacuum seal at the O-ring. The evacuation is ended and the specimen holder is removed from the airlock. During removal of the VTSH from the airlock, it is monitored for external radiation using an alpha meter. If no external contamination is detected, then surface swipes are made of the VTSH and counted with a alpha-beta counter to ensure that there is no removable contamination higher than background levels. During the contamination check procedures, the specimen sits under a static vacuum for approximately 10 minutes before the VTSH is taken to the TEM. During that time, the vacuum increases to ≈ 10 millitorr.

After the VTSH is approved for release from the radioactive materials laboratory, it is taken to the TEM, inserted into the airlock of the TEM, and moved into the TEM column, as with any other specimen holder. The tip of the specimen holder is un-retracted from the

VTSH into a standard specimen position in the TEM column. From this point on, transmission electron microscopy experiments are performed as usual.

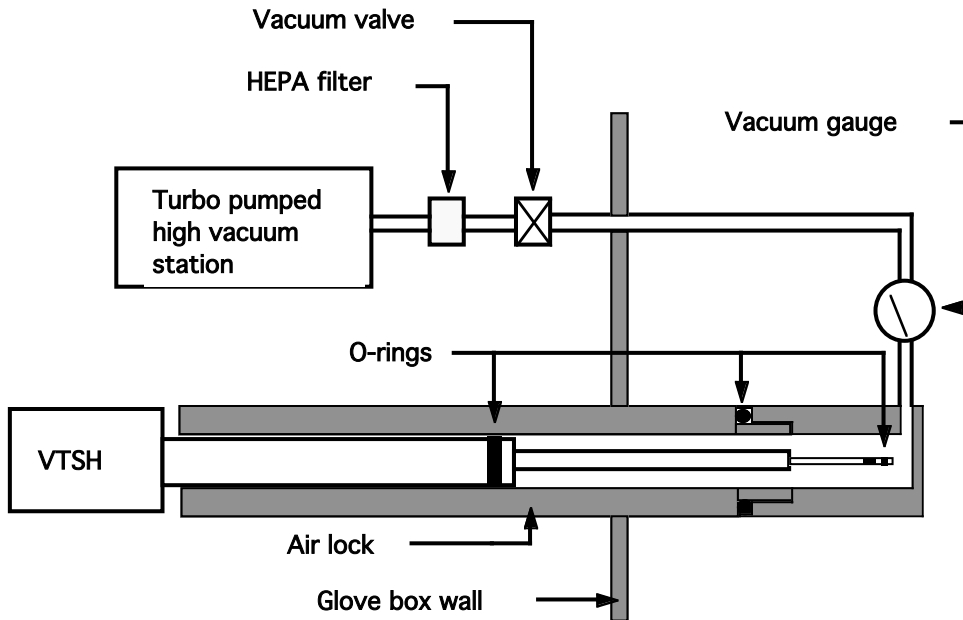


Figure 1. A drawing of the specimen holder airlock and evacuation system.

Experimental Samples

Specimens for TEM examination were extracted from eight separate sources of Pu-Ga alloys of ages 0.5, 16, 19, 26, 35, 36, 41, and 42 years. Special care was taken throughout the process to prevent any significant temperature rise or stress in the material and in the specimens extracted from it to assure that no phase transformations or microstructural changes were induced during TEM specimen preparation.

Transmission Electron Microscopy Observations

Conventional microscopy, even at very high magnification, is unable to resolve small bubbles or voids in the absence of a strain field. In order to observe these features, we employ the Fresnel imaging technique to observe surfaces in the under- and over-focus conditions.^{10,11} Figure 2 shows a through-focus series of TEM micrographs of He bubbles in a 42-year old material in a non-diffracting condition. The arrowed features in the $-1.4 \mu\text{m}$ under-focused image in Figure 2a appear as dark fringes surrounding a light dot. The same arrowed features in the $+1.4 \mu\text{m}$ over-focused image in Figure 2b appear as light

fringes surrounding a dark dot. There is no contrast associated with these features in the in-focus image due to an absence of strain fields (or the presence of very small strain fields) associated with the bubbles (Figure 2c). Even in a strongly diffracting condition, the bubbles are invisible when the image is in focus because the bubble diameter is much smaller than the extinction distance for the most common 2-beam imaging conditions.

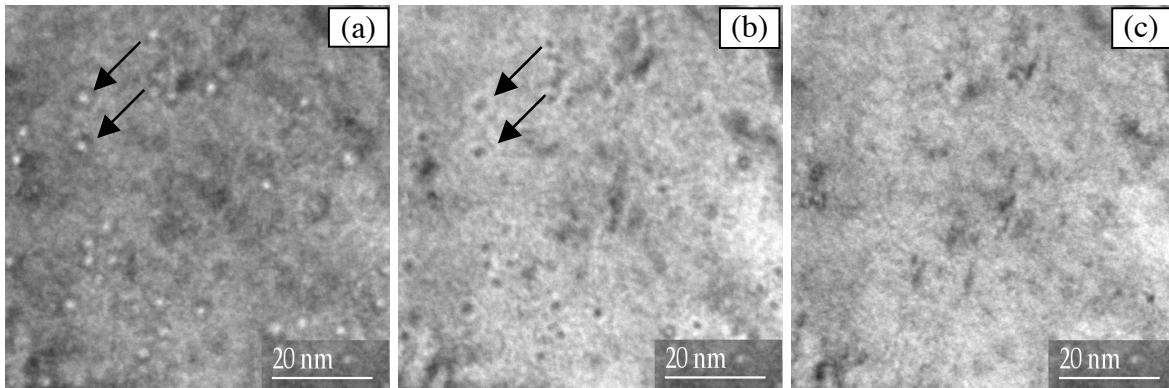


Figure 2. TEM images of 42-year old Pu alloy. (a) The $-1.4 \mu\text{m}$ under-focus bright-field TEM micrograph shows a high number density of very small helium bubbles as dark fringes surrounding a light dot; (b) The $+1.4 \mu\text{m}$ over-focus image reveals the bubbles as light fringes surrounding a dark dot, (c) The in-focus image does not reveal the presence of bubbles due to the absence of strain fields.

Stereo pair imaging¹² is applied to determine the distribution of bubbles and to confirm that these features are not surface artifacts induced by specimen preparation. In this technique, a unique surface feature is located and used as a fiducial mark. A small contamination mark in an approximately 20 nm thick sample is identified and labeled in Figure 3. The orientation of the specimen goniometer is recorded and a micrograph is taken. The specimen holder is then rotated approximately four degrees around the principal axis of the specimen holder (vertical axis in the micrograph) before a second micrograph is recorded. Analysis of the first image in Figure 3 reveals 15 bubbles; their x -distances from the fiducial mark are measured. The same bubbles are located in the second image, and again, the x -distances from the fiducial mark are measured. Simple geometry is used to determine the depths of the bubbles in the micrograph. The table in Figure 3

presents the results that clearly indicate the He bubbles are uniformly distributed throughout the thickness of the specimen.

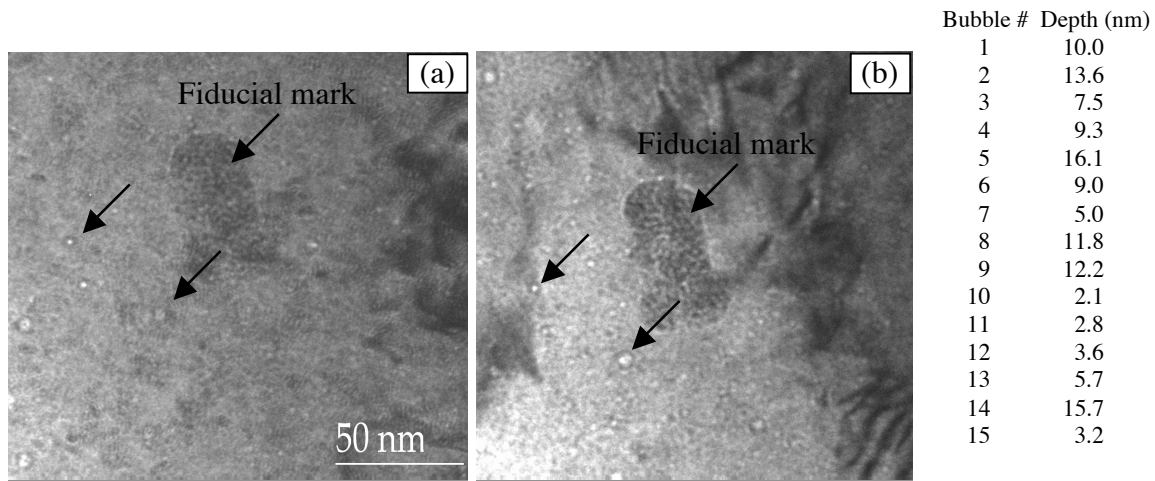


Figure 3. Stereo pair image of a 35-year-old material. The specimen thickness is approximately 20 nm. (a) TEM image recorded at 0° tilt, and (b) TEM image taken at 4° tilt. By measuring the change in distance from the fiducial mark, the depths of the He bubbles through the thickness of the specimen are determined and shown in the table on the right.

In addition to being uniformly distributed through the thickness of the Pu alloy specimens, He bubbles also appear to be distributed uniformly distributed throughout the interiors of the grains, as shown in Figure 4. Larger bubbles are visible at high angle grain boundaries and along the cores of dislocations, and are expected due to the enhanced helium diffusion rate in these areas. To determine the bubble diameters from the images, intensity scans are taken across the middle of the bubbles. The width at half maximum is the diameter used for the histograms of bubble sizes shown in Figure 5 and Table 1. The measurement and counting of bubbles is done from numerous micrographs taken in the under- and over-focus conditions. The greatest contribution to error in the measurement of number density is the uncertainty of the foil thickness. Both electron energy loss spectroscopy (EELS)¹³ and stereo pair imaging¹² have been used to determine the foil thickness of a number of samples. However, these techniques have not been applied to every region of the foil from which the bubble measurements were taken. On average, the EELS analysis and the stereo pair imaging result in foil thickness of approximately 40 nm,

and this is the value used to calculate the bubble number density and volume fraction for all the samples. The bubble density ranges from 0.6×10^{17} to $2.0 \times 10^{17}/\text{cm}^3$, but due to the uncertainty of the TEM specimen thickness, it could be as low as $1.2 \times 10^{17}/\text{cm}^3$ or as high as $2.5 \times 10^{17}/\text{cm}^3$. A lower value for the average diameter is 1.3 nm, giving a volume fraction of 0.0001. An estimate of the upper limit gives a volume fraction of 0.0003. Using an average number density of $1.8 \times 10^{17}/\text{cm}^3$ leads to an average inter-bubble spacing of 18 nm. The bubble number densities as determined by TEM of Pu alloys are similar to the density of helium bubbles in other materials. Brager and Garner¹⁴ report the observation of 2 nm helium bubbles with a number density of $1.7 \times 10^{17}/\text{cm}^3$ for irradiated type 316 stainless steel.

In contrast to bubble number densities, void number densities are expected to be lower by at least one to two orders of magnitude. Additional measurements using positron annihilation spectroscopy and theoretical analysis¹⁵ corroborate our identification of these cavities as helium bubbles with a helium to vacancy ratio of approximately two to three.

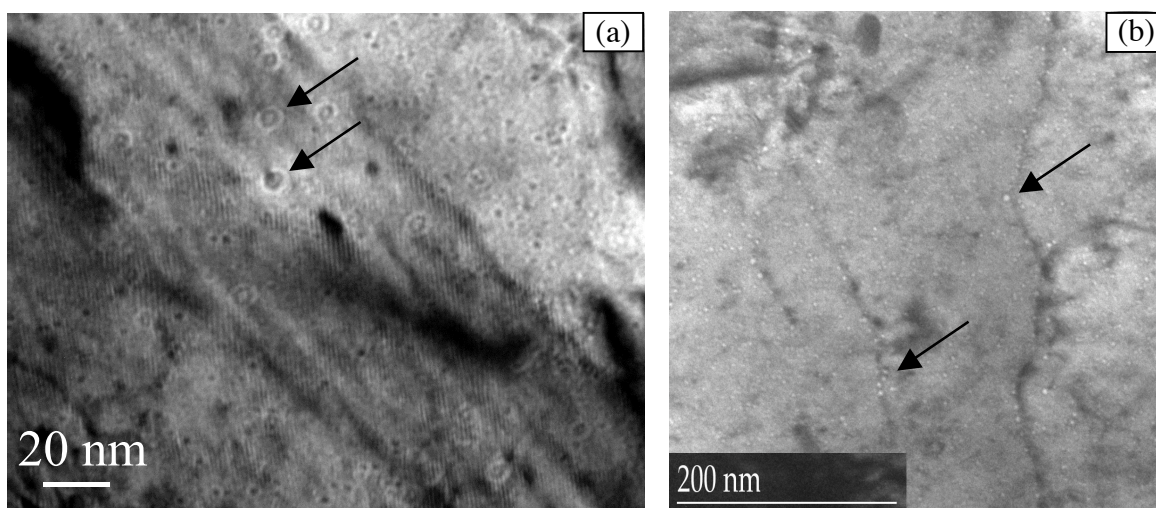


Figure 4. TEM images of a 42-year old Pu alloy. (a) Fresnel fringe image of bubbles on a highly inclined grain boundary reveals the bubble size to be approximately 3 times larger on the boundary than in the surrounding matrix, and (b) larger bubbles are observed on dislocation cores. Arrows indicate the locations of larger bubbles at grain boundaries and dislocation cores.

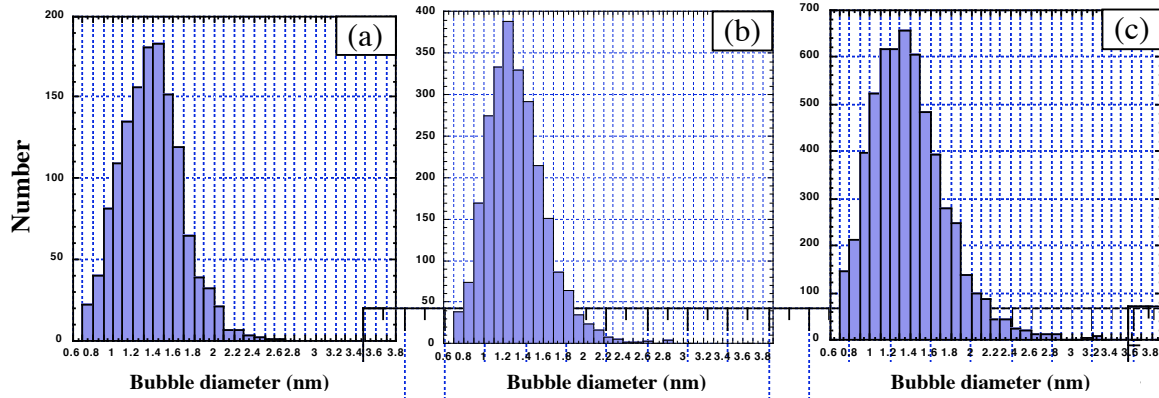


Figure 5. Histograms of He bubble distributions materials of three different ages. (a) 26-year old, (b) combined data from 35- and 36-year old, and (c) 42-year old material.

Table 1. Statistics of He bubble sizes and number densities.

Age (yrs)	Average diameter (nm)	Average # density ($\times 10^{17}/\text{cm}^3$)	Bubble volume fraction (%)
6 months	N/A*	N/A	N/A
16	1.4 ± 0.2	0.6 ± 0.3	0.01
19	1.4 ± 0.2	1.5 ± 0.4	0.02
26	1.3 ± 0.2	1.6 ± 0.4	0.02
35 and 36	1.3 ± 0.2	1.8 ± 0.4	0.02
41	1.6 ± 0.2	0.9 ± 0.3	0.02
42	1.4 ± 0.2	2.0 ± 0.4	0.03

*Bubbles smaller than ~ 0.7 nm are not resolved.

Summary

We have developed and demonstrated safe and technically sound procedures for preparing TEM specimens from Pu alloy samples. These procedures are very reproducible with the current success rate at approximately 70%. The amount of electron transparent area that can be observed is consistent with many other high atomic number and high-density materials and there does not appear to be major specimen preparation induced artifacts. The amount of oxide on the sample does appear to be related to the amount of time the specimen is exposed to various levels of reactive gases, i.e., O_2 and H_2O . With the current capabilities for producing Pu alloy TEM specimens under low-oxidizing conditions,

the oxide is not a limiting factor for imaging, diffraction, or spectroscopy experiments in the TEM. Finally, it should be noted that these types of sample preparation procedures are applicable to other materials that are highly reactive to O₂ and H₂O.

The self-irradiation in Pu by the alpha decay process is known to result in the formation of lattice damage and the generation of U and He atoms. We have identified three age-related phenomena due to self-irradiation in Pu alloys that may cause dimensional changes: the initial transient as a result of dislocation loop generation within collision cascades, helium accumulation, and void swelling. We have characterized Pu alloys ranging in age from 6 months to 42 years old with TEM and observed the presence of nanometer-sized helium bubbles. The average diameter of the bubbles in this age range varies from 1.3 to 1.6 nm and is observed to change very little with age beyond 16 years. The average number density of bubbles is in the range of 0.6×10^{17} to $2.0 \times 10^{17}/\text{cm}^3$ and appears to increase at a steady rate with time. No evidence of void swelling is observed in any of the materials.

Acknowledgments

The authors wish to thank Dennis Fleming, Rick Gross, Joe Magana, Bob McGee, and Larry Walkley of LLNL for their technical support. This work was performed under the auspices of the U.S. Department of Energy by the University of California, Lawrence Livermore National Laboratory under contract No. W-7405-Eng-48.

References

1. N. T. Chebotarev and O. N. Utkina, in *Plutonium 1975 and Other Actinides*, edited by H. Blank and R. Lindner (North Holland Publishing Co., Amsterdam, 1975), p. 559.
2. C. M. Schaldach and W. G. Wolfer, in *ASTM STP 1447*, edited by M. L. Grossbeck, T. R. Allen, R. G. Lott, and A. S. Kumar (ASTM International, West Conshohocken, PA, in press, 2004).
3. F. A. Garner, in *Materials Science and Technology: A Comprehensive Treatment*, Vol. 10A, Part I, edited by B. R. T. Frost (Wiley-VCH Verlag GmbH, Weinheim, Germany, 1994), p. 419-543.
4. W. G. Wolfer, *Los Alamos Science* **26**, 274-285 (2000).
5. B. D. Wirth, A. J. Schwartz, M. J. Fluss, M. J. Caturla, M. A. Wall, and W. G. Wolfer, *MRS Bulletin* **26**, 679 (2001).
6. R. H. Howell, P. A. Sterne, J. Hartley, and T. E. Cawan, *Applied Surface Science* **149**, 103 (1999).
7. D. L. Rohr, K. P. Staudhammer, and K. A. Johnson, *Los Alamos National Laboratory Report No. LA-9965-MS* (1984).
8. D. L. Rohr and K. P. Staudhammer, *Journal of Nuclear Materials* **144**, 202-204 (1987).

9. T. G. Zocco and D. L. Rohr, in *Specimen Preparation for Transmission Electron Microscopy of Materials*, edited by J. C. Bravman, R. M. Anderson, and M. L. McDonald (Materials Research Society Symposium Proceedings **115**, Pittsburgh, PA, 1988), pp. 259-264.
10. P. Hirsch, A. Howie, R. B. Nicholson, D. W. Pashley, and M. J. Whelan, *Electron Microscopy of Thin Crystals* (Butterworths, London, 1965).
11. M. Ruhle and M. Wilkens, *Crystal Lattice Defects* **6**, 129-140 (1975).
12. G. Thomas and M. J. Goringe, *Transmission Electron Microscopy of Materials* (John Wiley & Sons, New York, 1979).
13. T. Malis, S. C. Cheng, and R. F. Egerton, *Journal of Electron Microscopy Technique* **8**, 193-200 (1988).
14. H. R. Brager and F. A. Garner, *Journal of Nuclear Materials* **117**, 159 (1983).
15. R. H. Howell and P. Sterne, private communication (2002).